Electronic Supplementary Material (ESI) for Nanoscale.
This journal is © The Royal Society of Chemistry 2015

Supplementary Information

Gating of single molecule junction conductance by charge transfer complex formation.

Andrea Vezzoli[1], Iain Grace[2], Carly Brooke[1], Kun Wang[3], Colin J. Lambert[2], Bingqian Xu[3], Richard J. Nichols[1] and Simon J. Higgins[1*]

1. Department of Chemistry, Donnan and Robert Robinson Laboratories, University of Liverpool, Liverpool L69 7ZD, United Kingdom.
2. Department of Physics, Lancaster University, Lancaster LA1 4YB, United Kingdom.
3. College of Engineering & NanoSEC, University of Georgia, 220 Riverbend Road, Athens, Georgia GA 30602, U.S.A.

Contents

1. Synthetic procedures and characterisation of compounds.

Molecule **2** was synthesised following the procedure developed by Leary *et al.*[1] 1,4-Diethylbenzene was obtained from Sigma-Aldrich and used as received.

Oligothiophene **1c** was synthesised by Sonogashira coupling of 5,5''–dibromo–2,2':5',2''–terthiophene with 6-chlorohex–1–yne, followed by catalytic hydrogenation and substitution of the halogen with a thioacetate group.

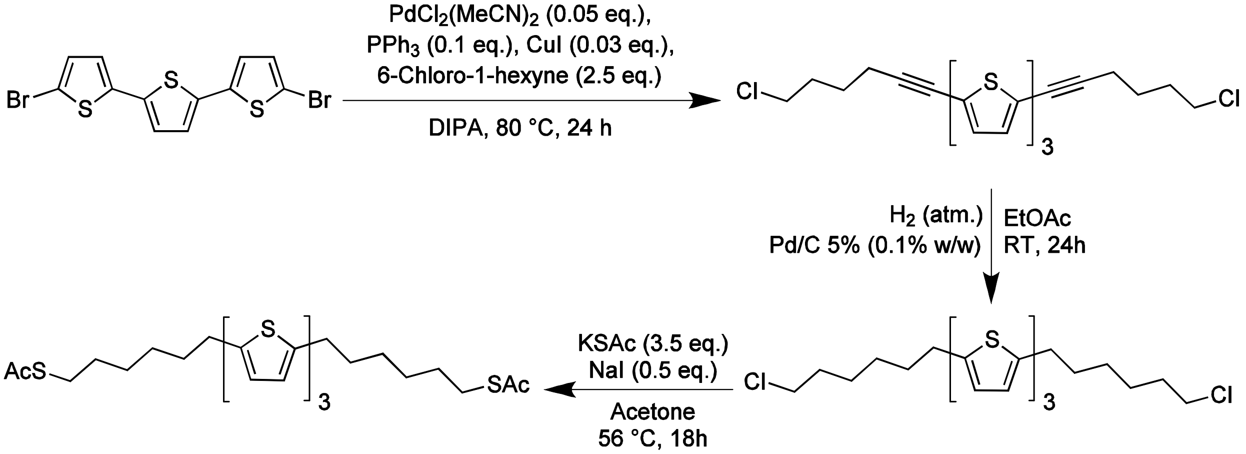

2,2':5',2''–Terthiophene was synthesised via Kumada coupling as reported in many literature sources,[2],[3] using [Ni(dppe)Cl_2] as catalyst. Bromination of 2,2':5',2''–terthiophene was performed using the procedure developed by Bäuerle *et al.*[4] Routinely, ^{1}H NMR was used to monitor the outcome of literature reactions. Reagents were purchased from Sigma-Aldrich Chemical Company and used as received, except where otherwise stated. Proton and ^{13}C NMR spectra were recorder using a Bruker Avance spectrometer and referenced to internal TMS. Mass spectra were recorded using a Carlo Erba 8000 Trio-1000 quadrupole spectrometer in CI positive ion mode (NH_3). High resolution mass spectra were recorded using a Waters Micromass LCT TOF spectrometer in ES+ (Na adduct) mode (CH_3OH).

1.1 Preparation of 5,5”-bis(6-chlorohex-1-ynyl)-2,2’:5’,2”-terthiophene.

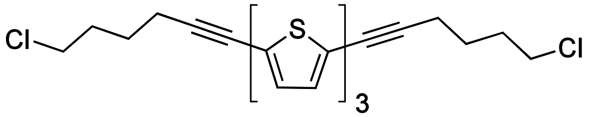

Diisopropylamine (50 mL) was degassed for 40 minutes by Ar bubbling prior to the addition of 5,5’’-dibromo-2,2’:5’,2’’-terthiophene (1.50 g, 3.69 mmol), [$PdCl_2(MeCN)_2$] (0.048 g, 5 mol %), PPh_3 (0.097 g, 10 mol %) and CuI (0.021 g, 3 mol %). After flushing with Ar for an additional 10 minutes, 6-chloro-hex-1-yne (1.155 g, 1.21 mL, 2.7 eq.) was added and the mixture was heated to 80°C under Ar and stirred for 16 hours. The resulting suspension was then allowed to cool down to room temperature and was filtered. The orange residue was triturated with petroleum ether, filtered again, washed with water and dried in vacuo to yield the title compound as bright yellow solid (1.12 g, 64 %). Found: C = 60.03, H = 4.60 %. $C_{24}H_{22}Cl_2S_3$ requires C = 60.37, H = 4.64 %. MS: m/z 477 [M^+]. ^{1}H NMR ($CDCl_3$, 400 MHz) δ = 1.78-1.94 (m, 8H), 2.50 (t, 4H, J = 7.0), 3.60 (t, 4H, J = 6.5), 6.98-7.01 (AB, 4H, J_{AB} = 3.8), 7.03 (s, 2H). ^{13}C NMR ($CDCl_3$, 100 MHz) δ = 19.1, 25.7, 31.7, 44.5, 74.3, 94.9, 123.0, 123.4, 124.6, 132.0, 136.0, 137.2.

1.2 Preparation of 5,5”-bis(6-chlorohexyl)-2,2’:5’,2”-terthiophene

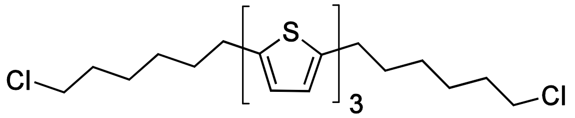

5,5”-bis(6-chlorohex-1-ynyl)-2,2’:5’,2”-terthiophene (0.630 g, 1.32 mmol) was subjected to catalytic hydrogenation (0.18 g 10 % Pd/C, H_2 atmosphere, 24 h, room temperature) in 50 mL of EtOAc. The catalyst was then filtered off through a bed of Celite and the solvent was removed in vacuo. The crude yellow solid was purified by flash column chromatography on silica (95:5 pet. ether 40-60:EtOAc) to yield the title compound as a bright yellow solid (0.43 g, 67 %). Found: C = 59.66, H = 6.10 %. $C_{24}H_{30}Cl_2S_3$ requires C = 59.36, H = 6.23 %. MS: m/z 485 [M^+]. ^{1}H NMR ($CDCl_3$, 400MHz) δ = 1.37-1.52 (m, 8H), 1.70-1.79 (m, 8H), 2.80 (t, 4H, J = 7.6), 3.53 (t, 4H, J = 6.7) 6.67 (d, 2H, J = 3.4), 6.96 (d, 2H), 6.97 (s, 2H). ^{13}C NMR ($CDCl_3$, 100 MHz) δ = 26.9, 28.6, 30.4, 31.8, 32.9, 45.4, 99.9, 123.6, 123.9, 125.3, 136.6, 143.8.

1.3 Preparation of 1 (S,S'-([2,2':5',2''-terthiophene]-5,5''-diylbis(hexane-5,1-diyl))diethanethioate)

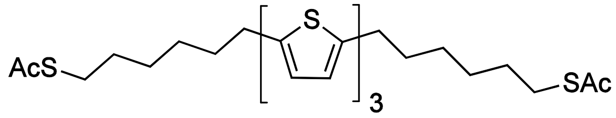

A solution of 5,5”-bis(6-chlorohexyl)-2,2’:5’,2”-terthiophene (0.363 g, 0.748 mmol), KSAc (0.263 g, 2.3 mmol) and NaI (0.011 g, 10 mol %) in acetone (50 mL) was refluxed under Ar atmosphere for 16 hours. The resulting brown suspension was filtered, the residue washed with cold acetone and the combined filtrates were concentrated in vacuo. The obtained crude product was purified by flash column chromatography on silica (CH_2Cl_2) and recrystallised from 30:70 CH_2Cl_2:40-60 pet. ether to give the title compound as a dull yellow solid (0.120 g, 28 %). Found: C = 59.32, H = 6.59 %. $C_{24}H_{22}Cl_2S_3$ requires C = 59.53, H = 6.42 %. MS: m/z 582 $[M+NH_4]^+$, 565 $[M+H]^+$. HRMS (ES+, MeOH, 45V) m/z 587.1220 $[M+Na]^+$. ^1H NMR ($CDCl_3$, 400MHz) δ = 1.39 (*broad* m, 8H), 1.58 (m, 4H), 1.67 (*broad* m), 2.32 (s, 6H), 2.78 (t, 4H, J = 7.4), 2.87 (t, 4H, J = 6.5) 6.66-6.95 (AB, 4H, J_{AB} = 3.5), 6.97 (s, 2H). ^{13}C NMR ($CDCl_3$, 100MHz) δ = 28.5, 28.6, 29.1, 29.4, 30.1, 30.7, 31.4, 123.2, 123.5, 124.9, 134.7, 136.1, 145.1, 196.2.

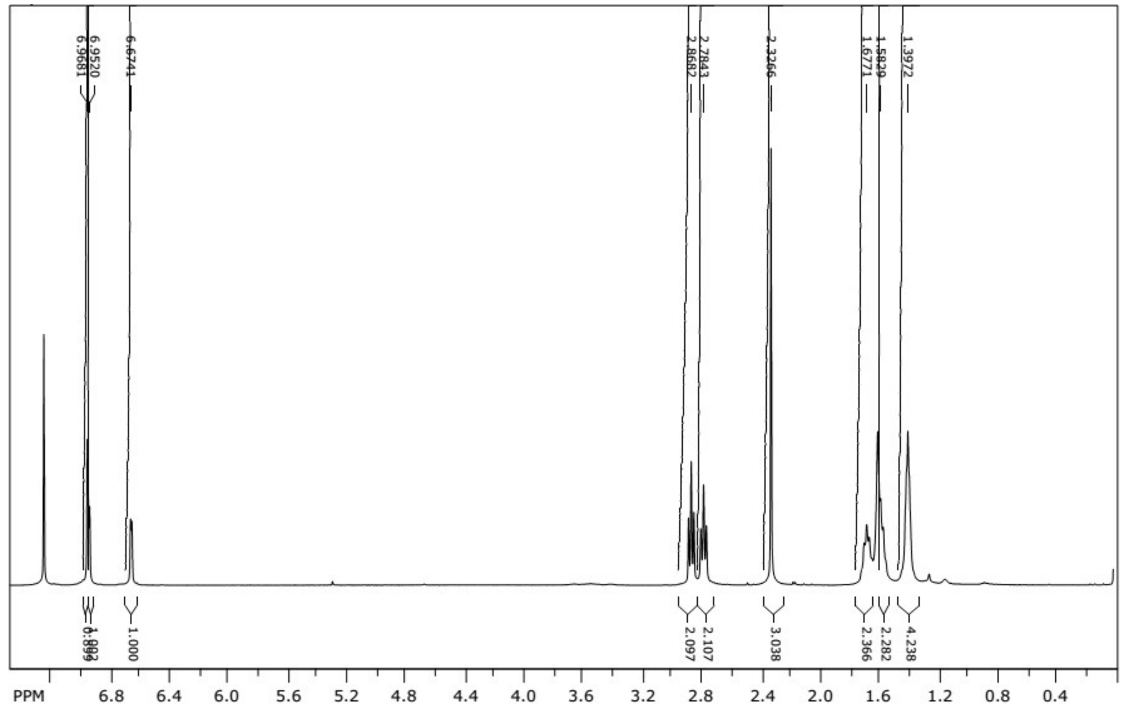

Figure S1: ^1H NMR (400 MHz, $CDCl_3$) spectrum of final compound **1c**

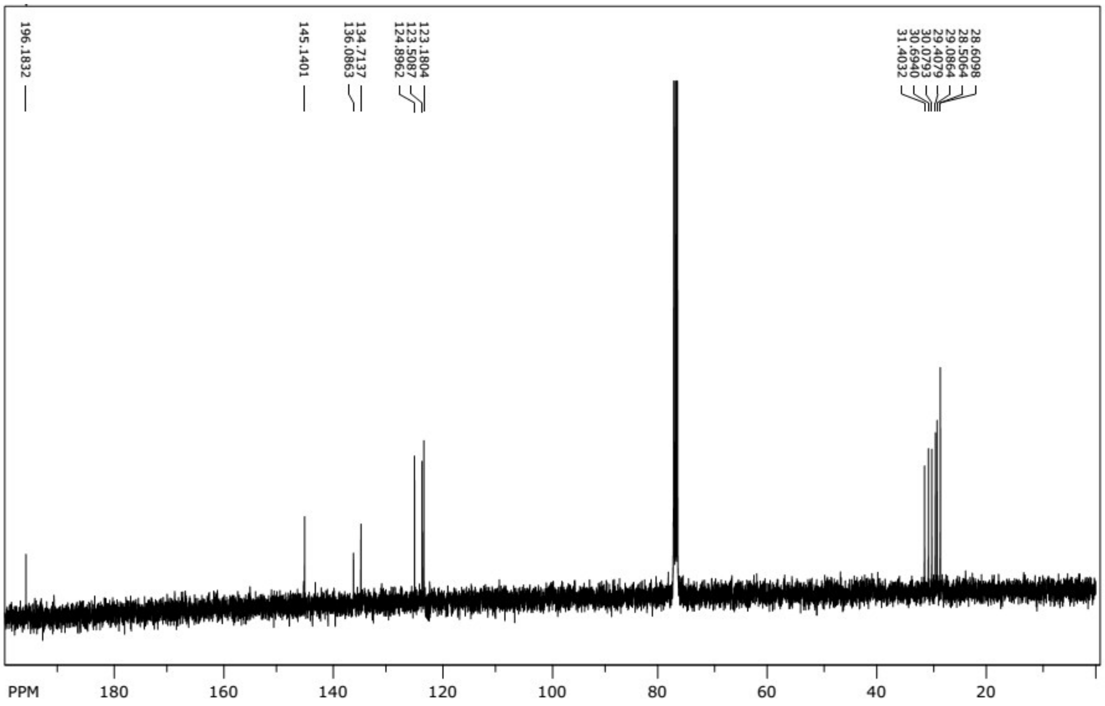

Figure S2: ^{13}C NMR (100 MHz, $CDCl_3$) Spectrum of final compound **1c**

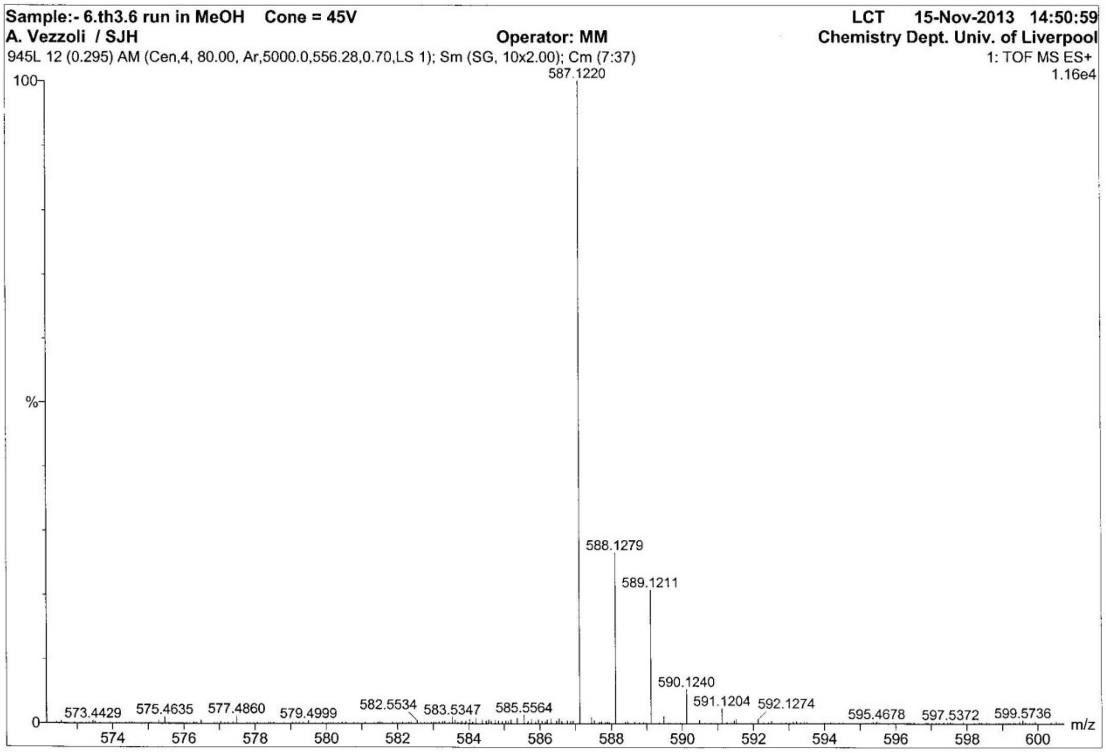

Figure S3: High resolution mass spectrum of final compound **1c**

2. Details of gold on glass sample preparation for STM-BJ measurements.

2.1 Molecule 1c and 1c:TCNE (Liverpool)

11 mm x 11 mm gold on glass samples (Arrandee GmbH, DE – 250 nm Au ¦ 2.5 nm Cr ¦ 0.7 mm borosilicate glass) were flame annealed with a Bunsen burner immediately prior to sub-monolayer deposition. The annealing process involves heating the sample held at ~45° in the flame until it glows red and then keeping it glowing for 10 s by moving it in and out of the flame. It is important to avoid overheating of the substrate as this will result in bent samples that can cause frequent tip crashes while doing STM measurements. The sample is then allowed to cool down for 30 s and the process is repeated three times. This procedure leads to the formation of atomically flat Au terraces, as can be seen in Fig. S4, which shows triangular (111) morphology[5] and one-atom deep step-like features (image rendered using Nanotech WsXM[6] software).

The sample is allowed to cool down to room temperature before further use in STM experiments.

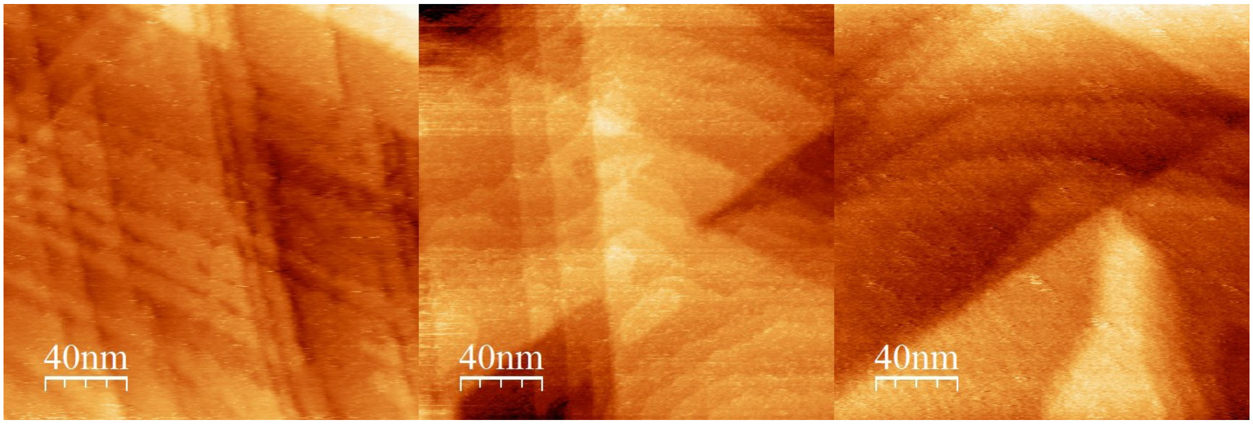

Figure S4: STM images (200x200 nm) of gold on glass samples after flame annealing

2.2 Molecule 2 and 2:TCNE (Georgia)

For the STM-BJ experiments performed on molecule **2**, the gold substrates were prepared by evaporating~100 nm of gold onto freshly cleaved mica sheets using a thermo-evaporator under a vacuum of 10^{-7} Torr. The gold beads for Au substrate deposition was purchased from Kurt J. Lesker Company (99.999%), and mica sheets were from Ted Pella, Inc. The Au surfaces were annealed in hydrogen flame for several minutes immediately before immersion in sample solutions of molecule **2**. This annealing step cleaned the surface and allowed epitaxial reconstruction of the Au to form large terraces of Au(111). Then sample solution containing target molecules was dropped onto the freshly flamed Au surface to form the required self-assembled monolayer for the conductance measurements, which were conducted in the absence of a liquid medium.

3. Additional details for single molecule junction experiments.

3.1 Description of methods

In order to determine molecular conductance and its dependence on the presence of TCNE an STM (former Molecular Imaging PicoSPM I, now 4500 SPM, Keysight Technologies Inc., USA) equipped with a freshly cut gold tip (Goodfellow Cambridge Ltd., UK - 99.99+%, 0.25mm), was used to form metal | molecule | metal junctions.

In the main paper we have focussed on results obtained using the in-situ STM-BJ method. This technique, originally developed by Xu and Tao[7] in 2003, involves the repeated formation of molecular junctions by pushing the gold tip into a gold surface (annealed as described in section 2) followed by retraction, in a solution of the desired molecular wire. Experiments on **1c** and its TCNE complex were performed in Liverpool and on **2** and its TCNE complex in Georgia.

In the Liverpool implementation of the technique, the tip is kept at a fixed distance from the surface (determined by the setpoint and bias voltage), driven towards the substrate to a negative height z of –2 nm, and then withdrawn at a constant speed (5 nm s^{-1}) while maintaining a constant x-y position. We observe current steps G_0 (77.4 μS) corresponding to the breaking of gold atomic chains,[7] and the subsequent smaller current steps characteristic of the breakdown of molecular junctions. During the withdrawal of the tip, a current-distance curve is collected. If a metal | molecule | metal junction forms, typically a characteristic shape is observed: the current (which is always larger than in the absence of a molecule) decreases with distance z and often settles at a plateau, typical of conductance through the extended molecule. It then abruptly decays to zero when the metal | molecule | metal junction is broken. Many (in this work, approximately 5000 for each set of conditions) of these current-distance curves are recorded and statistically analysed in histograms as described below. No data selection was employed; all traces, whether they contained an obvious plateau or not, contributed to the histogram plots. Experiments on the molecules in the absence of TCNE were conducted using 10^{-3} M solutions of **1** in 1,2,4-trichlorobenzene, while in experiments on doped molecular wires, solutions of 10^{-3} M molecular wire and 10^{-2} M TCNE were used. The noise level of this technique is usually between 10^{-6} and 10^{-5} G_0 [8] for our instrumentation and the bias voltages (experiments in main paper: 0.1 V) employed here, but in the presence of 10 mM TCNE, we noted a significantly higher current limit, probably due to a small Faradaic component due to the electroactive TCNE, since an uncoated tip was used.

The experiments on **2** were performed at Georgia also using the STM-BJ technique originally developed by Xu and Tao.[7] In this experiment, the STM tip was first driven into the gold substrate covered by desired molecules and then retracted away from the substrate, generating a current-distance curve during the tip retraction process. The STM tip engaged towards the Au substrate at a stop position controlled by a threshold tip-substrate current of 25 μA under a bias voltage of 0.3 V, plus an additional engage distance of 0.5 nm to ensure the physical contact between the tip and substrate. This setting guaranteed that all conductance traces displayed clear Au-Au point contact plateaus prior to the molecular plateaus. The tip engaging speed of 30 nm s^{-1} and retraction speed of 20 nm s^{-1} were used in the experiments. This process was repeated thousands of times to reveal thousands of curves that were subsequently used for the construction of conductance histogram. To prepare the samples, molecule **2** was first dissolved in the mixed solution of CH_2Cl_2 and ethanol (1:1 v:v) to give a 10^{-3} M solution of **2**. Molecule **2** solution was placed onto the freshly flamed Au surface and left for an incubation period of 15 minutes which led to the formation of a self-assembled monolayer of **2**. Then the sample surface was rinsed with ethanol and dried with high purity nitrogen gas. Conductance measurements for molecule **2** were subsequently conducted in air at room temperature (~20 ˚C). To form TCNE doped molecules, TCNE solution (10^{-2}M in CH_2Cl_2) was dropped onto the prepared monolayer of molecule **2** for a subsequent incubation period of 1 h. Then the sample was copiously rinsed with ethanol and dried with high purity nitrogen gas. Conductance measurements for doped molecular wires were also done in air at room temperature (~20 ˚C). In these experiments, the bias voltage was 0.3 V.

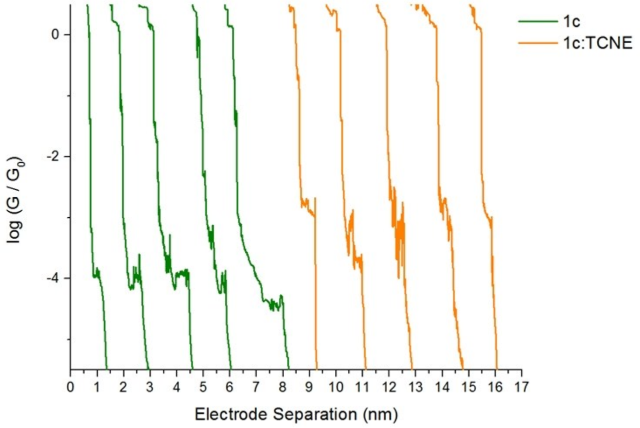

Figure S5. Example STM-BJ current traces for experiments on molecule **1c** alone (green), and in the presence of a 10-fold excess of TCNE (orange).

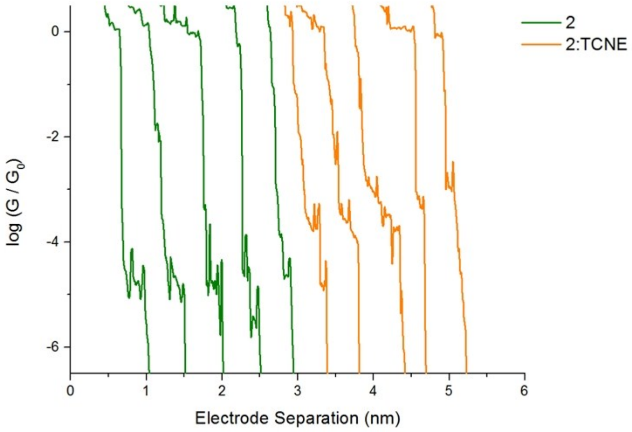

Figure S6. Example STM-BJ current traces for experiments on molecule **2** alone (green), and in the presence of a 10-fold excess of TCNE (orange).

3.2 Comparison of results from Liverpool and Georgia versions of STM-BJ methods.

Fig. S7 shows conductance histograms obtained using the Liverpool and Georgia implementations of the STM-BJ method for **1c** in the absence of TCNE, while Fig. S8 shows the data for **1c** in the presence of TCNE. Table S1 summarises the conductance values derived from these histograms.

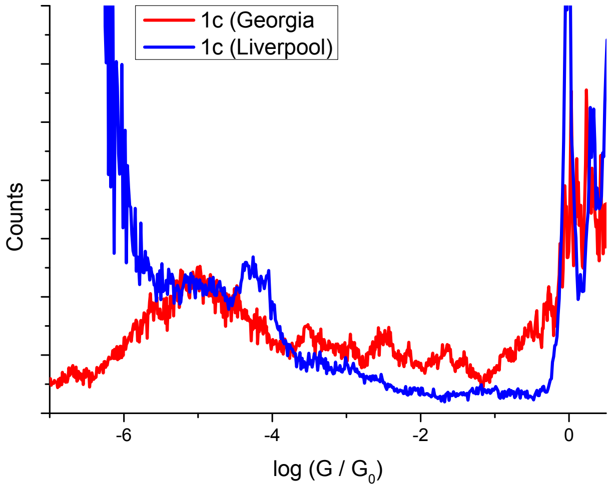

Figure S7. Conductance histogram for **1c** obtained in Liverpool (blue) and Georgia (red)

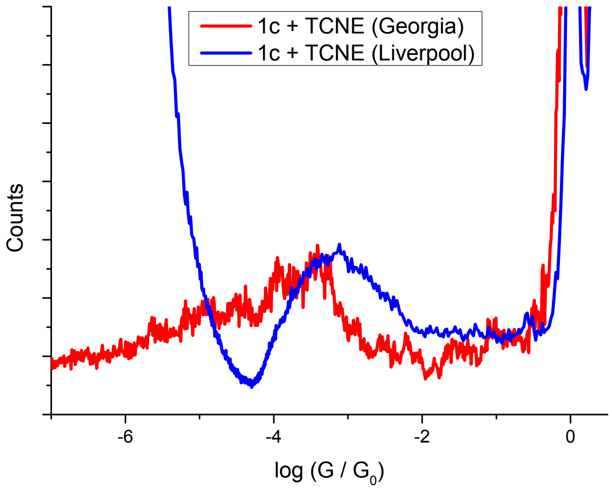

Figure S8. Conductance histogram for **1c**:TCNE complex obtained in Liverpool (blue) and Georgia (red)

It can be seen that the experiments performed in Liverpool gave slightly higher conductance values for both the isolated molecule and its complex, but the factor by which the conductance increases upon complexation with TCNE is reasonably consistent. The reasons for the conductance discrepancies are attributed to the different experimental conditions (1,2,4-trichlorobenzene as the medium for the experiments performed in Liverpool; air for the experiments performed in Georgia).

	1c	**1c + TCNE**	**Boost**
Liverpool	5.1 x 10^{-5} G_0	1.0 x 10^{-3} G_0	20x
Georgia	1.2 x 10^{-5} G_0	3.1 x 10^{-4} G_0	26x

Table S1: Comparison of data obtained in Liverpool and Georgia for molecule **1c** and its TCNE complex

As discussed in the main paper, we were unable to obtain meaningful conductance histograms for the **2:**TCNE complex in solution using the Liverpool implementation of the STM-BJ method, therefore only the data obtained in Georgia is presented and discussed in the paper.

3.3 Methods for the control experiments

We conducted control experiments in Liverpool in which we investigated the possibility of junction formation involving TCNE alone, and in which we measured the conductance of junctions using 1,10-decanedithiol in the presence and absence of TCNE. For these experiments, we used both the STM BJ method and additionally, we used the *I(s)* technique developed by Haiss et al.[9] In the latter technique, molecular adsorption is achieved by dipping gold-on-glass samples (flame-annealed as described in section 2) in a 10^{-4} M CH_2Cl_2 solution of the appropriate molecular wire. The tip is held above the surface at a desired setpoint current and bias voltage and then withdrawn at a speed of 40 nm s^{-1} while maintaining a constant *x-y* position. Again, during the withdrawal a current-distance curve is collected. If a molecule is present in the gap between the tip and the surface, a characteristic shape is observed in *I(s)* curves: the current decreases exponentially with the distance to settle at a plateau, typical of conductance through the extended molecule, and then it abruptly decays to zero when the metal | molecule | metal junction is broken. This technique differs from the *STM-BJ* technique as no physical contact between gold tip and gold substrate occurs prior to the formation the molecular junctions. The geometry of the STM tip will change less for the entire duration of these experiments than the STM-BJ technique since the tip is not pushed into the metallic substrate and this can promote greater reproducibility of single molecular junctions. Moreover, as the tip is maintained sharp, it is possible periodically to image the gold surface with high resolution. The noise level of this technique is usually between 10^{-8} and 10^{-7} G_0 with the bias voltages used here.

Conductance values are given as multiples of 10^{-6} G_0, where G_0 is the quantum of conductance, ≈77.4 µS. Conductance and standard deviation values were calculated from the raw experimental data using descriptive statistical algorithms (OriginPro9, OriginLab Corp., USA).

4. Control experiment: 1,10-decanedithiol in 1mM TCNE in TCB

For the *I(s)* control experiments on 1,10-decanedithiol, we manually selected data with at least one current plateau longer than 0.05 nm. As described in the literature current-distance traces with a plateau followed by a step are synonymous with the formation of molecular junctions. Because the *I(s)* technique is employed using a sub-monolayer coverage of molecules, the chance of forming a molecular junction (‘hit-rate’) is low, and therefore unselected data includes many traces where molecules are in the gap but unconnected at one (possibly both) end(s), and junctions which are unstable or noisy. By selecting data using a consistent procedure across all datasets we aim to exclude to a better extent traces where no proper junction forms which is important given the stochastic nature of junction formation.

Type-I, type-II and type-III transient curves have been observed during the *I(s)* experiments, and typical examples are presented in Fig. S9

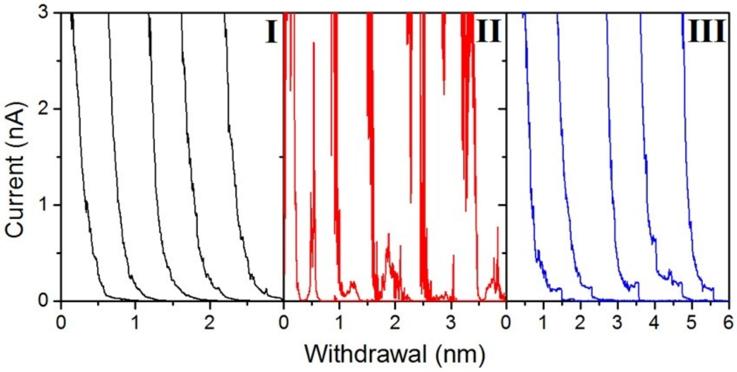

Figure S9: Typical *I(s)* traces observed during the control experiments. Type-I curves show smooth exponential decay. Type-II curves are non-monotonic and noisy. Type-III curves show step-like features as the tip is withdrawn. Curves obtained using 1,10-decanedithiol in TCB, using a tip bias of 0.3 V.

Type-I curves, showing smooth exponential decay, were observed in around 60% of the retraction events, and such curves show no sign of molecular junction formation, but simple electron tunnelling from the tip to the substrate. Type-II curves are noisy and non-monotonic, and have been attributed again to noise or impurities in the gap between the two metallic leads. The percentage of these noisy curves is around 30%. Type-III curves (about 10 % of retraction events), showing exponential decay followed by step-like features (plateaux) and abrupt decay have been attributed to conductance through the molecular backbone in Au | molecule |Au junctions. Note that the *I(s)* technique gives a lower percentage of Type-III curves than the in-situ BJ technique; this is understandable bearing in mind that the heavy contact where the tip is pushed into the surface is avoided. Only type-III curves have been collected (300-800 for each experiment) for the *I(s)* control experiments, and used to construct conductance histograms in the experiments on 1,10-decanedithiol (DDT). The same traces were used to compose 2-dimensional density plots, accounting for the experimentally determined tip-sample separation (z_0) before tip withdrawal as explained later.

	Literature in Air (10^{-6} G_0)[10]	**DDT in TCB (10^{-6} G_0)**	**DDT 2mM TCNE in TCB (10^{-6} G_0)**
Conductance[a]	7.59 ± 1.15	7.47 ± 2.06	8.11 ± 1.41

Table S2: Single molecule conductance values of **DDT** in different media.

The conductance of junctions with 1,10-decanedithiol were measured in TCB and in 1mM TCNE in TCB to rule out possible interactions of TCNE with the Au surface and/or the sulfur contacts. Results and literature values are reported in Table S2 and conductance histograms are reported in Fig. S10.

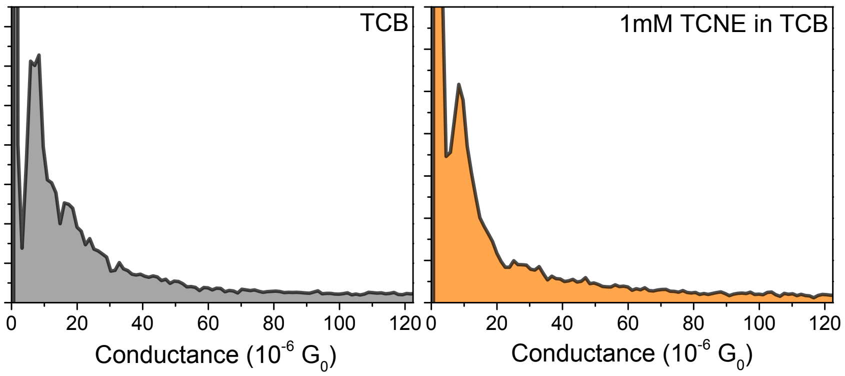

Figure S10: Conductance histograms of **DDT** in pure TCB (left)
and 1mM TCNE in TCB (right).
Experimental conditions: *I(s)* technique, 10 nA setpoint, 0.3 V tip bias.

5. UV-Vis Characterisation of TCNE complexes

UV-Visible spectrometry has been used to characterise the formation of TCNE complex of **1** and diethylbenzene (DEB - as surrogate for **2**) in organic solution (CH_2Cl_2). Spectra were recorded on a double beam Perkin Elmer Lambda 25 spectrometer, operating in the region 50000-9000 cm^{-1}, using a 1 cm quartz cell at room temperature. Spectra are shown in Fig. S11-12.

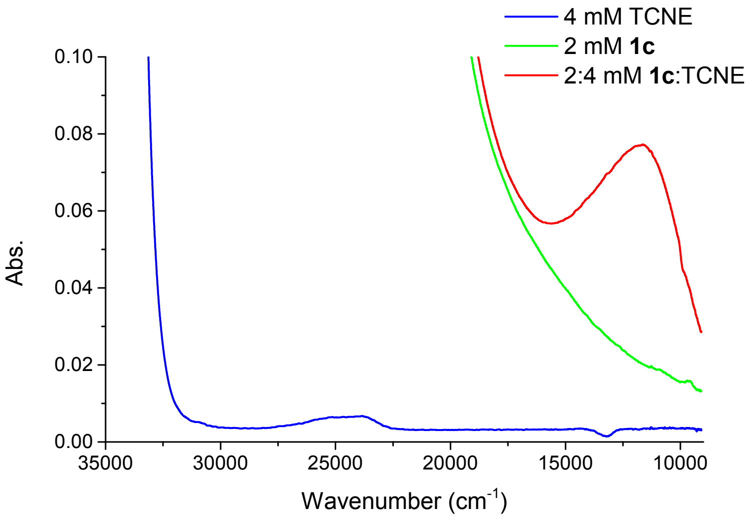

Figure S11: UV-Vis spectrum of **1c**:TCNE complex compared with the corresponding spectra of its individual components.

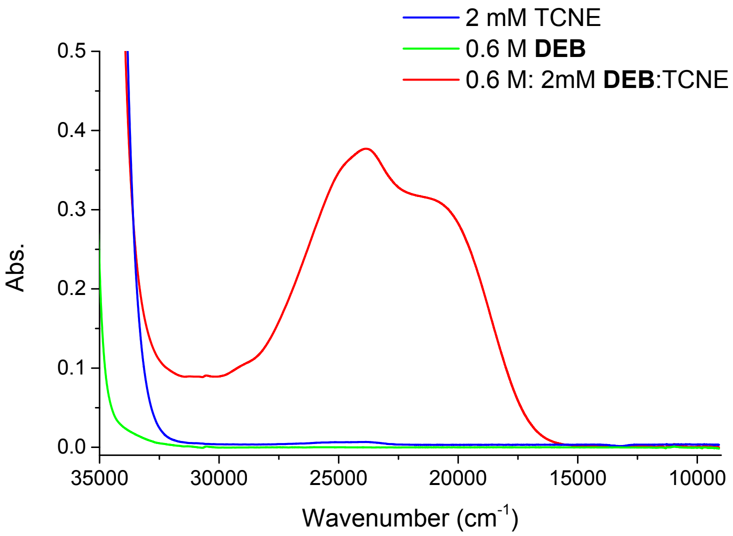

Figure S12: UV-Vis spectrum of **DEB:TCNE** complex compared with the corresponding spectra of its individual components.

The donor-acceptor interaction of complex DEB:TCNE has been analysed quantitatively using the Benesi-Hildebrand[11] procedure:

$$\frac{[TCNE]}{A_{CT}} = \frac{1}{\varepsilon_{CT}} + \frac{1}{K_{DA}\varepsilon_{CT}[DEB]}$$

Where A_{CT} is the molar absorbance of the charge transfer complex, ε_{CT} is the extinction coefficient of the charge transfer band at the monitoring wavelength ($\lambda_{MAX} = 23800$ cm^{-1} – 420 nm) and K_{DA} is the association constant for the formation of the complex in solution. A plot of **[**TCNE**]**/A_{CT} *vs* 1/**[**DEB**]** is linear as can be seen in the inset of Fig. S13 and the least-squares fit produced a correlation coefficient of 0.998. From the slope $[K_{DA}\varepsilon_{CT}]^{-1}$ and the intercept $[\varepsilon_{CT}]^{-1}$, the values for the association constant and the extinction coefficient were readily extracted as $K_{DA} = 2.7$ M^{-1} and $\varepsilon_{CT} = 500$ M^{-1} cm^{-1}.

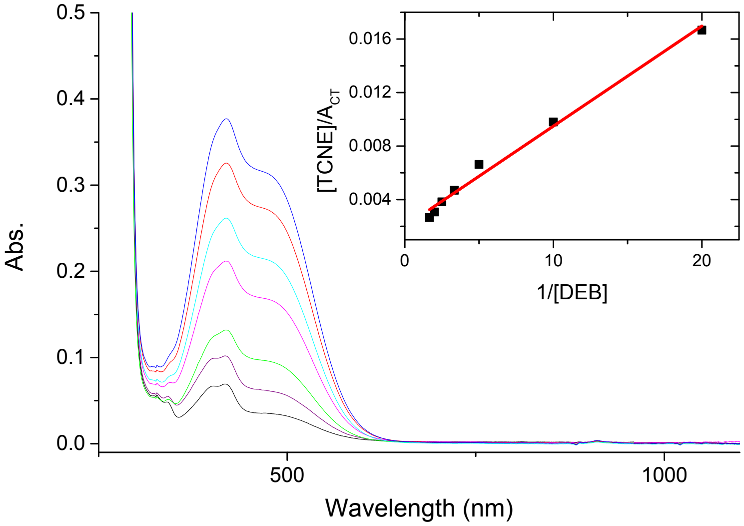

Figure S13: Spectral (UV-Vis) changes attendant upon the incremental addition of DEB to TCNE. Inset: Benesi-Hildebrand plot. [DEB] = 0.0495, 0.099, 0.198, 0.297, 0.396, 0.495 and 0.594 M. [TCNE] 1.01 mM.

It should be noted that the Benesi-Hildebrand method is an approximation, and is only valid where the minority species (in this case, TCNE) is largely complexed, and where the CT band of the complex is in a spectral region where none of the other components of the mixture absorbs.[12] If we discard the point where [DEB] is lowest (and hence the first criterion is least likely to be met), then the slope and intercept change, such that ε_{CT} becomes 1000 dm^3 mol^{-1} cm^{-1} and K_{DA} becomes 1. This is much closer to the values for the DEB:TCNE complex in CH_2Cl_2 previously published.[13] We were unable to determine K_{DA} and ε in this manner for **1c:**TCNE since, as can be seen in Fig. S9, the CT absorption partly overlaps with the low-energy side of the terthiophene π-π* absorption.

6. **Theoretical methods**

The geometry of molecules **1c** and **2** can have a significant effect on the predicted theoretical conductance, due to the presence of the alkane chains and their orientation with respect to the central unit. To find the optimum geometry, 60 different starting orientations were chosen and each system was relaxed using density functional theory. The lowest-energy configuration was then taken to be the geometries for **1c** and **2**. The molecules were relaxed with the SIESTA code, using a double- ζ plus polarization orbitals basis set until all the forces on the atoms were less than 0.01 eV/Ang. The local density approximation was used for the exchange correlational functional, with norm conserving pseudopotentials and a cutoff of 150 Rydbergs describing the real-space grid.

To calculate the conductance through molecules **1c** and **2**, an extended molecule approach was taken, with 6 layers of (111) gold each containing 9 gold atoms added to each side. The binding locations of the terminal sulfur atoms were taken to be top sites, with a gold sulfur distance of 2.5 Angstroms. The zero-bias transmission coefficient *T(E)* was then calculated using the SMEAGOL code. These simple lead structures enable efficient calculation of numerous configurations of the TCNE-molecule complex.

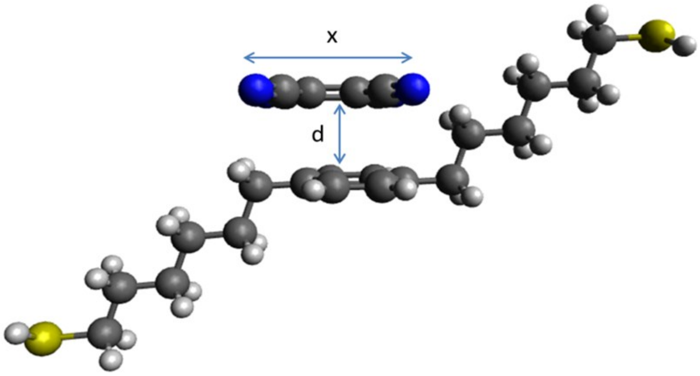

Figure S14: Optimum configuration for TCNE bonded to molecule **2**.

To calculate the structure of the TCNE-molecule complex, starting from the relaxed geometry of both molecules the TCNE molecule was moved along locations surrounding the central unit of the molecule (see Figure S12) until a minimum energy position was located by optimizing the binding energy. The resulting conformation is a pi-stacking arrangement, in which the TCNE molecule is located a distance d above the central unit and is displaced laterally by a distance x relative to one end of the central unit. The range of values is taken to be 2.7 Å $< d <$ 3.7 Å and $0 < x < 7.5$ Å for **1** and $0 < x < 1$ Å for **2**. In total the binding energies for 500 configurations were calculated. The optimum geometry can be seen for **1c** in Fig. 5 of the main paper and for **2** in Fig. S14. To compute the binding energy, the ground state energy of the total system (which is a dimer) is calculated using SIESTA. For these calculations we use the vdw functional to describe the exchange correlation due to the fact that LDA can underestimate the binding energy in pi-stacked systems. The ground state energy of the dimer is defined as E_{AB}^{AB}. The energy of each monomer is then calculated in the total basis, which is achieved through the use of ghost atoms in SIESTA. Hence the energy of the individual TCNE in the presence of the total basis is defined as E_{A}^{AB} and for the isolated molecule is E_{B}^{AB}. The binding energy ΔE is then calculated using the following equation:

$$\Delta E = E_{AB}^{AB} - E_{A}^{AB} - E_{B}^{AB}$$

The resulting energy landscapes can be seen in Fig. S15 which consist of a series of mimima at positions along each molecule's backbone. For each of these 500 configurations the transmission coefficient was calculated and these are shown in Fig S.16.

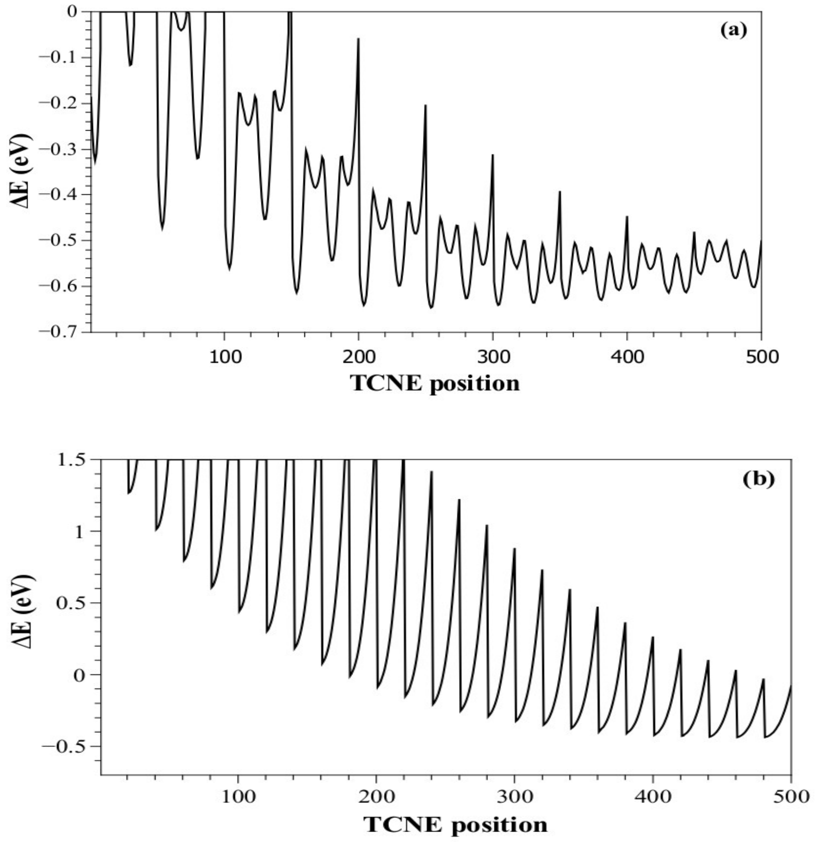

Figure S15. Binding energy for a TCNE molecule on (a) molecule **1c** and (b) molecule **2** for 500 different binding locations.

The Fano resonances seen in the transmission coefficients arise when extended states of the molecular junction (including the gold contacts) interact with a bound state. In the examples of Fig. 5 in the paper, the bound state is an orbital of the TCNE, part-filled by the charge transfer interaction. Since TCNE is a strong electron acceptor, the position of this orbital automatically adjusts to achieve the required filling and is therefore almost independent of the location and orientation of the TCNE relative to the backbone. Furthermore, since a part-filled orbital must be necessarily located near to the Fermi energy E_F, it is natural to expect the Fano resonance to be located near E_F and therefore the transmission coefficient $T(E_F)$, which largely determines the electrical conductance, should be strongly affected. It is well known that DFT cannot accurately predict the true position of the Fermi energy E_F relative to molecular orbitals within a junction and therefore Fig. 5 only shows the location of the Fano resonance relative to the 'bare' E_F^0. To locate E_F, we computed the electrical conductance $G = I/V$ at finite voltage V, where

$$I = \left(\frac{2e}{h}\right)\int \int_{-\infty}^{\infty} dE < T(E) > (f_+(E) - f_-(E))$$

, for a range of values of E_F, where $<T(E)>$ is the average of all curves shown in Fig. S14 and $f_{+/-}(E)=1/(exp(E-E_F +/- eV/2)/k_BT +1)$ is the Fermi function of the left (+) or right (-) electrode. The right-hand panel of Fig. 5 shows that for a Fermi energy lying in the HOMO-LUMO gap, an enhancement of 27-fold (compared with the conductance in the absence of TCNE) occurs at E_F-E_F^0 = +0.20 eV (dashed line). This is close to the experimentally observed enhancement factor of 20. This suggests that the experimental Fermi energy E_F is close to, but not equal to, the bare DFT value E_F^0. Fig. 6 in the main paper shows the corresponding theoretical data for **2** which predicts a lower conductance enhancement of 15.

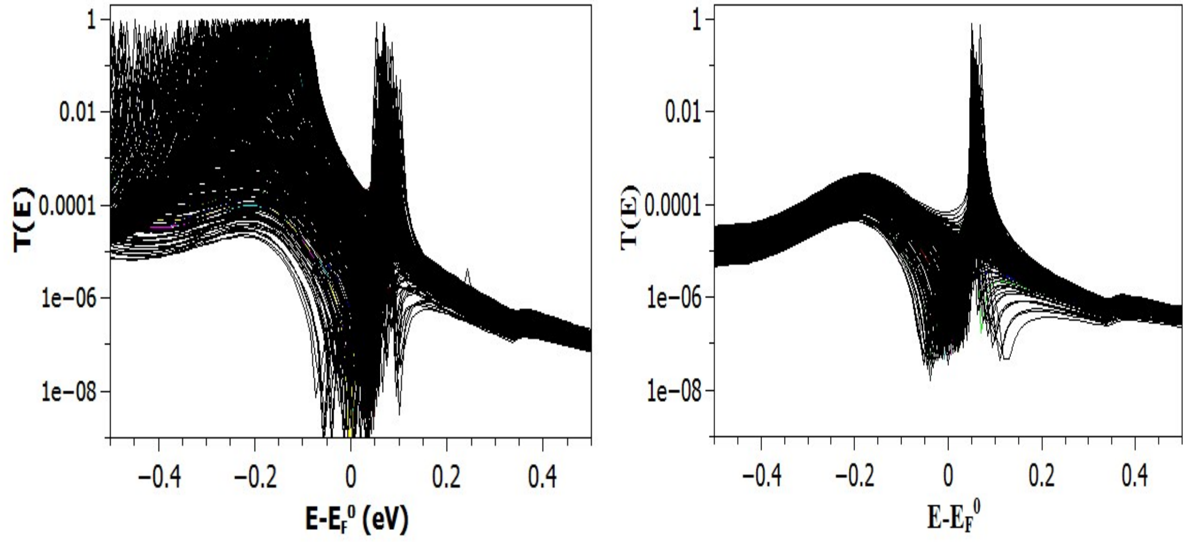

Figure S16. Transmission coefficients for each of the 500 binding locations for molecules **1c** (left) and **2** (right).

Fano resonance at the Fermi Energy

The results in the main paper show that the presence of the TCNE molecule produces a Fano resonance close to the Fermi Energy, which does not appear for the non-complexed molecule. This is attributed to charge transfer from the backbone molecule onto the TCNE. To study this effect in more detail we evaluate the local density of states (LDOS) of the molecular junction and perform a population analysis of the charge.

A Fano resonance arises due to interaction between a bound state that it weakly coupled to the continuum state, which in this case is an orbital located on the TCNE molecule. To show this more clearly we plot the LDOS around the Fermi energy for the transmission curve shown in Figure 5 of the main text. Figure S17(a) shows the contour plot of LDOS in blue between energies of –0.15 and –0.05 eV; here the LDOS is located mainly on the thiol anchor groups and corresponds to the small peak in the transmission curve. S17(b) is the LDOS at the Fermi energy (0 eV) evaluated between –0.05 and 0.05 eV and clearly shows a strong weighting on the TCNE molecule, therefore in this energy range there is an orbital located on the TCNE molecule. Finally S17(c) is the LDOS between 0.4 and 0.5 eV; this is in the middle of the HOMO-LUMO gap and the LDOS is located mainly on the gold electrodes.

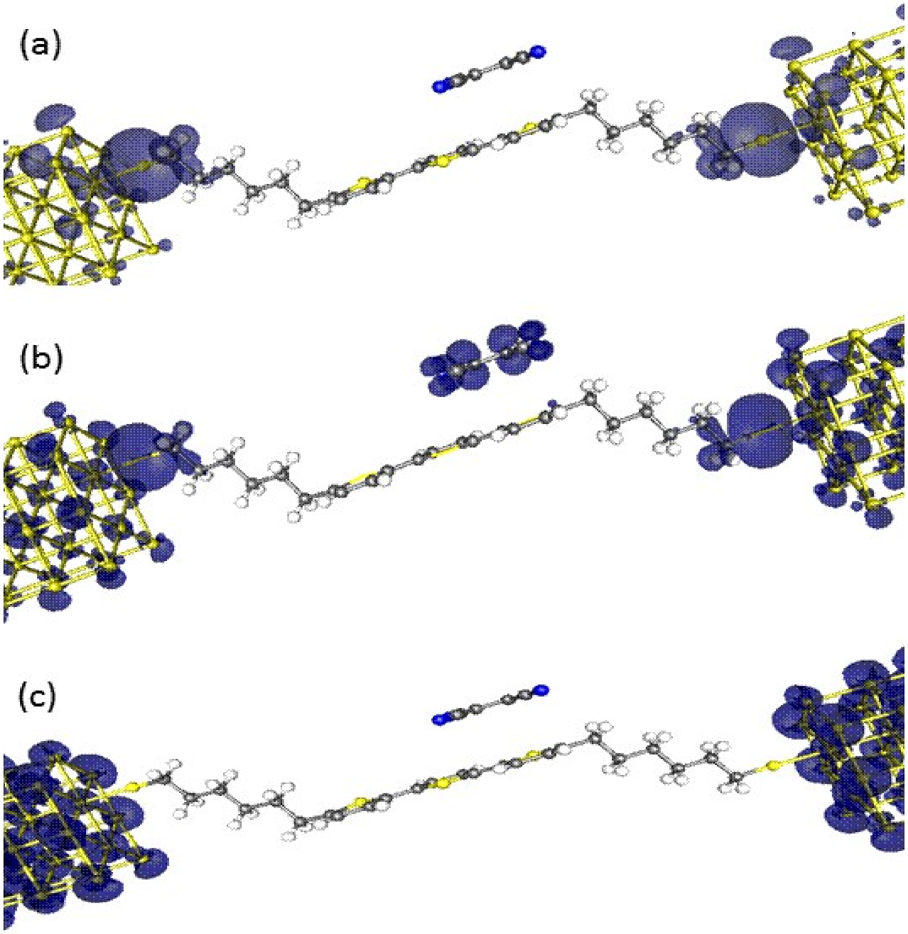

Figure S17. Local density of states (LDOS) for three different energy ranges: (a) –0.15 to –0.05 eV, (b) –0.05 to 0.05 eV and (c) 0.4 to 0.5 eV, where 0 eV is the Fermi energy.

Mulliken and Bader charge analysis

To show that charge is transferred from the backbone molecule to the TCNE acceptor molecule, we perform a population analysis of the charge on the TCNE molecule within the junction using the SIESTA code. The results for the charge on each atom within the TCNE molecule can be seen in Figure S18 below. The results show for both methods that the TCNE gains charge upon charge transfer complex formation with **1c**, as neutral uncomplexed TCNE should have 44 valence electrons; both Mulliken and Bader give similar values.

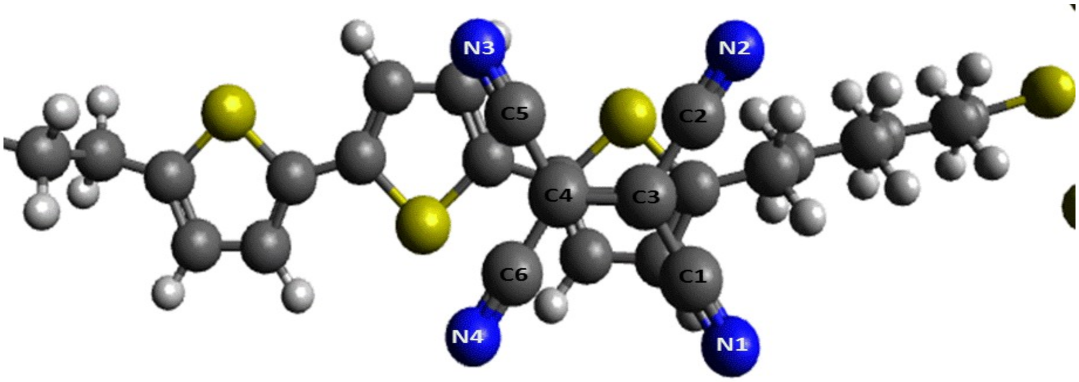

	Mulliken	Bader
N1	5.6294	4.743
N2	5.5718	4.741
N3	5.5893	4.729
N4	5.6864	4.735
C1	3.5156	4.341
C2	3.6622	4.342
C3	4.022	3.975
C4	3.7793	3.968
C5	3.3639	4.344
C6	3.4684	4.344
Total	44.2883	44.262

Figure S18. Mulliken and Bader charge population on each atom of the TCNE molecule within the molecular junction

Increasing the separation of the charge transfer complex

Figure S19 shows the evolution of the Fano resonance in the transmission coefficient *T(E)* as the distance *d* between the backbone molecule and the TCNE (Fig S14) is increased from 3.2 to 5.2 Å. As *d* is increased, the coupling between the two molecules decreases and the Fano resonance becomes narrower. At a distance of 5.2 Å the coupling due to the overlap of the orbitals has become zero and the Fano resonance accordingly disappears.

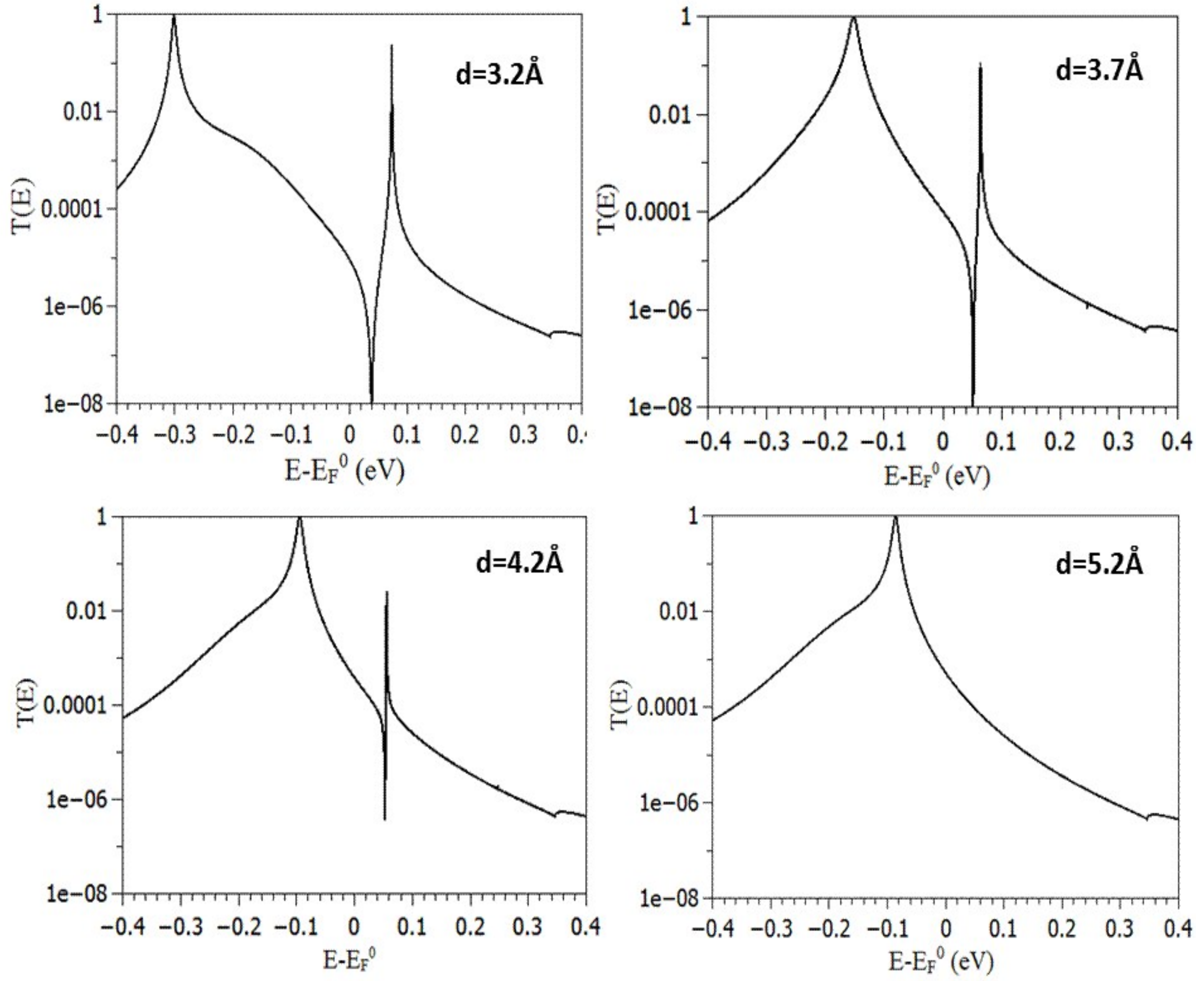

Figure S19. Transmission coefficient *T(E)* for different values of d shown in Figure S14.

References

1. E. Leary, S. J. Higgins, H. van Zalinge, W. Haiss and R. J. Nichols, *Chem. Comm.*, 2007, 3939-3942.
2. A. Carpita, R. Rossi and C. A. Veracini, *Tetrahedron*, 1985, **41**, 1919-1929.
3. B. J. J. Smeets, R. H. Meijer, J. Meuldijk, A. J. M. Vekemans and L. A. Hulshof, *Org. Process Res. Dev.* , 2003, **7**, 10-16.
4. P. Bäuerle, F. Würthner, G. Götz and F. Effenberger, *Synthesis*, 1993, **11**, 1099-1103.
5. H. Zhang, H. Li and Z. Liu, *Microelec. Eng.* , 2002, **63**, 381-389.
6. I. Horcas, R. Fernandez, J. M. Gomez-Rodriguez, J. Colchero, J. Gomez-Herrero and A. M. Baro, *Rev. Sci. Instrum.*, 2007, **78**, 013705.
7. B. Q. Xu and N. J. Tao, *Science*, 2003, **301**, 1221-1223.

8. W. Hong, H. Valkenier, G. Meszaros, D. Z. Manrique, A. Mishchenko, A. Putz, P. M. Garcia, C. J. Lambert, J. C. Hummelen and T. Wandlowski, *Beilstein J. Nanotech.*, 2011, **2**, 699-713.
9. W. Haiss, H. van Zalinge, S. J. Higgins, D. Bethell, H. Höbenreich, D. J. Schiffrin and R. J. Nichols, *J. Am. Chem. Soc.*, 2003, **125**, 15294-15295.
10. W. Haiss, S. Martin, L. E. Scullion, L. Bouffier, S. J. Higgins and R. J. Nichols, *Phys. Chem. Chem. Phys.*, 2009, **11**, 10831-10838.
11. H. A. Benesi and J. J. Hildebrand, *J. Am. Chem. Soc.*, 1949, **71**, 2703-2707.
12. M. J. S. Dewar and C. C. Thompson, *Tetrahedron*, 1966, **22 Supplement 7**, 97-114.
13. J. E. Frey, A. M. Andrews, D. G. Ankoviac, D. N. Beaman, L. E. Du Pont, T. E. Elsner, S. R. Lang, M. A. Oosterbaan Zwart, R. E. Seagle and L. A. Torreano, *J. Org. Chem.*, 1990, **55**, 606-624.